# Modeling and Studying the Impact of Dynamic Reactive Current Limiting in Grid-Following Inverters for Distribution Network Protection

Reynaldo S. Gonzalez, Venkatanaga A. Aryasomyajula, Krishna S. Ayyagari,
Nikolaos Gatsis, Miltiadis Alamaniotis, and Sara Ahmed
Department of Electrical and Computer Engineering, The University of Texas at San Antonio

***Abstract*—The growing use of renewable energy sources such as wind and solar in distribution networks (DNs) poses a challenge for DN protection. Inverter-based resources (IBRs) have fault responses that differ from conventional generators, which can have a significant impact on how the DN is protected and lead to misoperations, such as blinding. Use of simplified inverter models may result in incorrect relay settings and relay misoperations. This paper leverages a comprehensive grid-following inverter with dynamic reactive current (DRC) limiting model. The inverter with DRC model is combined with distribution system equations, to form a nonlinear differential and algebraic equations (NDAE) model, in which the fault response is verified. The grid-following inverter with DRC limiting is then implemented in a distribution system with protection elements and compared with a simplified fault response model based on frozen control. The system is tested under varying irradiance conditions, as well as varying dynamic factor $K$ of the DRC limiting model. The effect of the DRC current limiting model on protection blinding is investigated as well. The case study reveals that precise modeling of the PV inverter including the DRC limiter is indeed required to properly identify and predict blinding scenarios in the DN.**

***Keywords*—Dynamic reactive current, grid-following inverter, nonlinear differential and algebraic equations, overcurrent relay, protection**

## I. Introduction

Modeling of power electronics inverters with current limiting strategies is important for understanding the transient fault response of the network, ensure system protection, and avoid relay misoperations. With the recent integration of inverter-based resources (IBRs) into the distribution network (DN), traditional protection systems can face challenges in maintaining safe and reliable operation of the grid. IBR integration affects the fault currents of the system due to limited inverter current contribution during faults [1], and causes bidirectional current flows that impact the protection system. In addition, if there is a large number of inverters integrated into the DNs, the increase in fault current may cause misoperation of the protective devices [2], particularly overcurrent relays (OCR), which are typically used in DNs to protect from faults [3]. The OCR continuously monitors the current and if the current exceeds the specified setpoint, called pickup setting, the relay sends a trip signal to the circuit breaker. Greater penetration of IBRs can reduce upstream fault currents below the pickup setting, causing blinding misoperations [4], which is the focus of the present study. In addition to greater IBR penetration, PV irradiance, which varies throughout the day, may also cause significant changes in fault currents and this effect is also investigated in this work. Accurate fault analysis is required to determine OCR settings, thus modeling of the inverter and its fault response, is of great importance for protection studies considering distribution networks with IBRs.

Modeling of grid-following inverter controls includes the phase-locked loop (PLL), LCL filter, power controller, and current controller generally designed in the $dq$ (direct-quadrature or synchronous) reference frame [5]–[8]. The works in [5]–[8] do not include fault studies, however they focus on the dynamical models of inverter control and the response to step disturbances resulting from inverter power commands. Model nonlinearities are bypassed by linearizing the nonlinear equations around an equilibrium point. Also, the aforementioned works do not place particular emphasis on the distribution network and how the bus voltages, which amount to algebraic states of the network, vary when IBRs are integrated. In [9], although the nonlinearities in the IBRs integrated DN are considered, the developed model only studies dynamic stability under relatively small disturbances, such as a trip of lines, and step change in loads. In addition, the work in [9] mentions that the proposed model cannot be used to perform short circuit analysis. The short circuit response of inverters and their current limiting capability have been previously studied; see e.g., [1], [10]–[15]. The fault current contribution from inverters is typically limited to 1.2–1.5 times the rated current. Although studies on inverter short circuit contribution exist, such as the ones mentioned previously, most of these works lack in standardizing the inverter model and current limiting strategies for fault studies. In general, during faults, the inverter must provide fault current as a function of the terminal voltage at the point of common coupling (PCC). Specifically, the dynamic reactive current (DRC) limiting model for the inverter postulates reactive current injection which is proportional to the voltage deviation from the nominal voltage during the fault [16]. The proportionality between the inverter reactive current injection and the voltage deviation

This project and the preparation of this paper were funded in part by monies provided by CPS Energy through an Agreement with The University of Texas at San Antonio. This material is based upon work supported by the National Science Foundation under Grant CAREER-1847125.
Emails: (reynaldo.gonzalez, venkatanagaamrusha.aryasomyajula, krishnasandeep.ayyagari, nikolaos.gatsis, miltos.alamaniotis, and sara.ahmed)@utsa.edu.

at the PCC is defined by the dynamic factor $K$. While the current limiting of inverters has been modeled and studied, the applicability of such models for fault studies, and by extension for protection studies, are recently receiving wider attention. For example, the optimization based solver developed in [12] performs short-circuit analysis of inverter-integrated DNs but only considers a constant current source model for the inverter. CYME distribution analysis software, recently introduced a nonlinear inverter fault response model in version 9.3, whereas previous versions contained only constant current and voltage source behind impedance models. Studying the effect of inverter nonlinear models on protection systems is a growing area of interest, explained more in the next paragraph.

There are studies which investigate phenomena such as harmonic pollution [17], fault impedance [18], and transformer inrush [19], and their effects on overcurrent protection. Similarly, the effect of IBRs on network protection is a growing research area, but with respect to dynamic current limiting and OCR-based protection, it is not yet very well studied. The work in [11] studies the impact of IBRs on protection but lacks insight on the impact to OCRs and blinding misoperations. The fault response of solar DERs is explored in [10], but very little focus is placed on the protection. The work in [20] investigates the effect of negative sequence current injection on impedance-based protection, compared to conventional generators. The effect of nonlinear IBR fault models on incremental quantities-based protection is studied in [21]. The aforementioned papers study the effect of nonlinear IBR models on certain protection elements, however, the effects of the PV inverter dynamic current limiter on OCRs for DN, considering varying solar irradiance, as well as varying dynamic factor $K$, remains a desired study topic.

This paper develops a detailed nonlinear differential and algebraic equation (NDAE) model of a grid-following inverter interacting with a distribution system. Commercial simulation tools are usually limited to one inverter model with a few control types, as well current limiting strategies which cannot be modified by the user. When compared to commercial simulation, the NDAE model allows any different inverter model and control, as well as fault limiting strategies and can be tested on different distribution networks. A detailed DRC control and limiter model is incorporated together with legacy short-circuit response characterized by frozen control for comparison purposes. The grid-following inverter model also includes a PLL, LCL filter, power controller, and current controller. Subsequently, this paper leverages the detailed grid-following inverter model, which is extended to include a PV system, to present an analysis of blinding misoperations in protection systems.

The contributions of this work are summarized as follows:

- Development of a comprehensive NDAE model that includes distribution system dynamics and a grid-following inverter with DRC limiting.
- Simulation of balanced faults with the NDAE model on a 5-bus distribution system using MATLAB's ordinary differential equations (ODE) solver and comparison with the Simulink model.

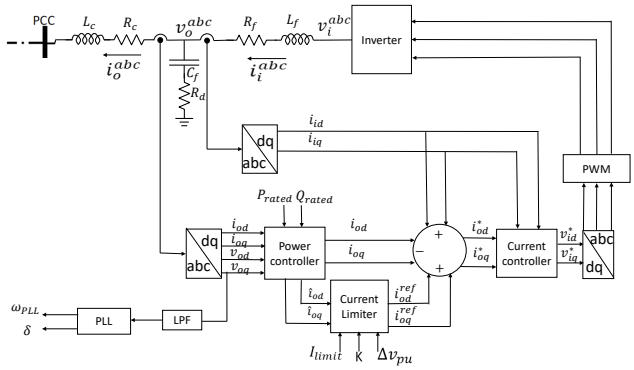


Fig. 1. Grid following inverter schematic.

- Simulink implementation of grid-following inverter for a solar PV system, connected to 5-bus distribution system with protection elements.
- Study of the effect of DRC limiting model on protection blinding while considering varying solar irradiance and different $K$-factor of the DRC limiter.

## II. NDAE Modeling of the Inverter-Integrated Distribution System

Consider an $n$-bus, 3-phase distribution system modeled as a tree network with set of edges denoted by $\mathcal{E}$. Bus-1 (root node) is the slack bus. The inverter is connected to a bus designated as the point of common coupling (PCC) through an LCL filter. In this work, we leverage the dynamics of the grid-following inverter model depicted in Fig. 1 represented in a local $dq$ synchronous reference frame. The dynamics of the rest of the system (that generically includes loads, transformers, and lines) are represented in a global synchronous reference frame $DQ$. The transformation angles the define the respective synchronous reference frames are given in the sequel. The overall system dynamics depend on the dynamics of the inverter combined with the current limiting strategy, as well as the connected load, transformer, and distribution lines between them. The various elements of the NDAE model are presented next.

### A. Inverter

In this section, the detailed analytical model of the inverter and its controls including the current limiting strategies are developed.

#### 1) Phase-Locked Loop (PLL)

The PLL is necessary to measure the actual frequency of the system. This work adopts a $dq$-based PLL [5]. The PLL synchronizes the estimated frequency $\omega_{\text{PLL}}$ to the grid synchronous frequency and produces the angle $\delta$ for the $dq$ transformation. The PLL aligns the $d$ or $q$ axis to the measured voltage and correspondingly sets $v_{oq}$ or $v_{od}$ to zero upon synchronization. In this paper, it is assumed that the PLL will set $v_{od} = 0$ at steady-state. The equations pertaining to the

PLL block are

$$\dot{v}_{od,f} = \omega_{c,\mathrm{PLL}} v_{od} - \omega_{c,\mathrm{PLL}} v_{od,f} \tag{1a}$$
$$\dot{\Phi}_{\mathrm{PLL}} = -v_{od,f} \tag{1b}$$
$$\omega_{\mathrm{PLL}} = \omega_n - k_{p,\mathrm{PLL}} v_{od,f} + k_{i,\mathrm{PLL}} \Phi_{\mathrm{PLL}} \tag{1c}$$
$$\dot{\delta} = \omega_{\mathrm{PLL}} - \omega_n \tag{1d}$$

where $v_{od,f}$ is the filtered $d$-axis voltage component; $\omega_{c,\mathrm{PLL}}$ is the cut-off frequency of the PLL low-pass filter; $\Phi_{\mathrm{PLL}}$ is an auxiliary state; $\omega_{\mathrm{PLL}}$ is the estimated PLL frequency; $\omega_n$ is the nominal grid synchronous frequency; $k_{p,\mathrm{PLL}}$ and $k_{i,\mathrm{PLL}}$ are the gains of the PI controller. The dynamic state vector corresponding to the PLL block is $\boldsymbol{x}_{\mathrm{PLL}} = \left[v_{od,f}, \Phi_{\mathrm{PLL}}, \delta\right]^T$.

*2) LCL filter*

The LCL filter in Fig. 1 consists of the filter inductance $L_f$, filter capacitance $C_f$, filter resistance $R_f$, the coupling inductance $L_c$ and resistance $R_c$, and a damping resistor $R_d$. The differential equations are obtained by applying Kirchoff's voltage law (KVL) between nodes at the input, output, and filter capacitor branches of the LCL filter in Fig. 1. The KVL equations in phase domain ($abc$) are converted to $dq$ frame using the transformation discussed in [22, Ch. 3] to yield the equations pertaining to the LCL filter as follows [5]

$$\dot{i}_{id} = \frac{1}{L_f}(v_{id} - v_{od} - R_f i_{id}) + \omega_{PLL} i_{iq} \tag{2a}$$
$$\dot{i}_{iq} = \frac{1}{L_f}(v_{iq} - v_{oq} - R_f i_{iq}) - \omega_{PLL} i_{id} \tag{2b}$$
$$\dot{i}_{od} = \frac{1}{L_c}(v_{od} - v_{\mathrm{PCC},d} - R_c i_{od}) + \omega_{PLL} i_{oq} \tag{2c}$$
$$\dot{i}_{oq} = \frac{1}{L_c}(v_{oq} - v_{\mathrm{PCC},q} - R_c i_{oq}) - \omega_{PLL} i_{od} \tag{2d}$$
$$\dot{v}_{od} = \frac{1}{C_f}(i_{id} - i_{od}) + \omega_{PLL} v_{oq} + R_d(\dot{i}_{id} - \dot{i}_{od}) \tag{2e}$$
$$\dot{v}_{oq} = \frac{1}{C_f}(i_{iq} - i_{oq}) - \omega_{PLL} v_{od} + R_d(\dot{i}_{iq} - \dot{i}_{oq}) \tag{2f}$$

where $i_{idq}$ are the $dq$ frame input currents of the filter. Assuming that the system is lossless, we consider that the commanded voltages $v^*_{idq}$—depicted as outputs of the current controller in Fig. 1 and discussed in Section II-A5—appear at the input of the filter inductor, that is, $v^*_{idq} = v_{idq}$. The output currents and the output voltages of the inverter in $dq$ frame are denoted as $i_{odq}$ and $v_{odq}$, respectively. The voltages $v_{odq}$ are fed back to the power controller for the reference currents calculations (cf. the next section). The bus voltages at PCC are defined as $v_{\mathrm{PCC},dq}$. The PCC will be any bus $j = 2, \ldots, n$ of the network where an IBR is connected to. The dynamic state vector for the LCL filter block is defined as $\boldsymbol{x}_{\mathrm{LCL}} = \left[i_{id}, i_{iq}, i_{od}, i_{oq}, v_{od}, v_{oq}\right]^T$.

*3) Power Controller*

The power controller regulates the output power by computing the output current references $i^*_{odq}$ based on feedback from the output voltages $v_{odq}$ using the instantaneous power theory [1]. The equations pertaining to the power controller are

$$\hat{i}_{od} = \frac{2}{3}\frac{1}{v_{od}^2 + v_{oq}^2}(v_{od} P_{\mathrm{ref}} + v_{oq} Q_{\mathrm{ref}}) \tag{3a}$$
$$\hat{i}_{oq} = \frac{2}{3}\frac{1}{v_{od}^2 + v_{oq}^2}(v_{oq} P_{\mathrm{ref}} - v_{od} Q_{\mathrm{ref}}) \tag{3b}$$

where $P_{\mathrm{ref}}$, $Q_{\mathrm{ref}}$ are the real and reactive power reference set points. The outputs of the power controller are as follows

$$i^*_{od} = i_{id} + \hat{i}_{od} - i_{od} \tag{4a}$$
$$i^*_{oq} = i_{iq} + \hat{i}_{oq} - i_{oq} \tag{4b}$$

Under faulted conditions, the current references $\hat{i}_{odq}$ need to be adjusted, as described next.

*4) Current Limiter*

To protect the power electronics from damage due to over voltage or over currents during faults, the inverter output current should be limited. The current references produced by the power controller [cf. (4)] are not applied during faults and the inverter acts like a current source subject to the following current limiting strategies:

- **Frozen control**: In this current limiting strategy, the inverter remains connected to the system and continues to feed its pre-fault output current, i.e, $i^{\mathrm{ref}}_{odq} = i_{odq,\mathrm{prefault}}$.
- **Dynamic reactive current control**: The inverter remains connected to the network and injects reactive current to the system. First, the inverter rated current is defined as $I_{\mathrm{rated}} = \frac{\sqrt{P^2_{\mathrm{rated}} + Q^2_{\mathrm{rated}}}}{\sqrt{3} V_{\mathrm{PCC,LL,rated}}}$, where $V_{\mathrm{PCC,LL,rated}}$ is the rated line-to-line voltage at the PCC. During faults, the inverter has the capability to provide current larger than its rated value by a factor typically in the range of 1.2–1.5. In the present paper, the maximum injected current during faults is defined as $I_{\mathrm{limit}} = 1.2 I_{\mathrm{rated}}$.

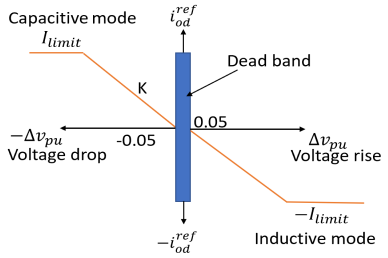


Fig. 2. Grid code requirement for reactive current injection during faults.

Typical grid code requirement for positive-sequence reactive current ($i_{od}$) injection is shown in Fig. 2. The premise is to ensure that inverters contribute reactive current during faults, with the purpose of providing voltage support. The per-unit change in terminal voltage at the PCC is $\Delta v_{\mathrm{pu}} = \frac{\sqrt{v^2_{\mathrm{PCC},d} + v^2_{\mathrm{PCC},q}} - V_{\mathrm{nom}}}{V_{\mathrm{nom}}}$, where $V_{\mathrm{nom}} = \frac{V_{\mathrm{PCC,LL,rated}}}{\sqrt{3}}$. When $\Delta v_{\mathrm{pu}}$ is within $\pm 5\%$ (cf. the deadband in Fig. 2), the inverter does not alter the current references computed by the power controller, that is, $i^{\mathrm{ref}}_{odq}$ will take the values calculated in (4). When the per-unit voltage deviation at the PCC $\Delta v_{\mathrm{pu}}$ is outside of the deadband, the inverter injects positive sequence

reactive current proportionally to $\Delta v_{\rm pu}$. The slope is denoted by dynamic factor $K$ in Fig. 2. The reactive current injection is

$$i_{\rm reactive} = i_{od,\rm prefault} - K\Delta v_{\rm pu}\sqrt{2}I_{\rm rated} \tag{5a}$$

$$i_{od}^{\rm ref} = \min\left\{\max\left\{i_{\rm reactive}, -\sqrt{2}I_{\rm limit}\right\}, \sqrt{2}I_{\rm limit}\right\} \tag{5b}$$

where the factor $\sqrt{2}$ accounts for the transformation from phase frame quantities ($I_{\rm rated}$ and $I_{\rm limit}$) to $dq$ frame quantities ($i_{od}$) following the $dq$ transformation definition given in [22, Ch. 3]. Eq. (5a) adjusts the pre-fault reactive current reference (if non-zero) by adding a component that follows the requirement of Fig. 2. Eq. (5b) projects the reactive current reference to respect the limit given by $I_{\rm limit}$.

The available active current injection is given by

$$i_{oq}^{\rm ref} = \text{sign}(\hat{i}_{oq})\min\left\{|\hat{i}_{oq}|, \sqrt{(\sqrt{2}I_{\rm limit})^2 - (i_{od}^{\rm ref})^2}\right\} \tag{6}$$

Eq. (6) prescribes that the active current reference produced by (4b) either remains unchanged or it is reduced so that together with $i_{oq}^{\rm ref}$ the current limit is respected. The output currents $i_{odq}^{\rm ref}$ are given as the input to the current controller to calculate the commanded voltages $v_{idq}^*$ as discussed next.

*5) Current Controller*

The current controller takes the difference between the output currents $i_{odq}^{\rm ref}$ obtained after applying the current limiting strategy and the input currents of the filter to calculate the commanded voltages $v_{idq}^*$. The dynamic equations that describe the behavior of the current controller include the state variables $\gamma_{dq}$ as follows

$$\dot{\gamma}_d = i_{od}^* - i_{id} \tag{7a}$$

$$\dot{\gamma}_q = i_{oq}^* - i_{iq} \tag{7b}$$

The outputs of the current controller are defined as

$$v_{id}^* = -\omega_n L_f i_{iq} + k_{ic,d}\gamma_d + k_{pc,d}\dot{\gamma}_d + v_{od} \tag{8a}$$

$$v_{iq}^* = \omega_n L_f i_{id} + k_{ic,q}\gamma_q + k_{pc,q}\dot{\gamma}_q + v_{oq} \tag{8b}$$

where $k_{ic,dq}$ and $k_{pc,dq}$ are the gains of the PI controller. The outputs $v_{idq}^*$ of the current controller appear at the input of the LCL filter, i.e., $v_{idq} = v_{idq}^*$. The dynamic state vector corresponding to the current controller block is defined as $\boldsymbol{x}_{\rm CC} = \left[\gamma_d, \gamma_q\right]^T$.

Next, the equations for source, transformer, line, and load in the global synchronous reference frame $DQ$ are discussed.

### B. Source

The slack bus is a positive sequence voltage source denoted as $v_{1,abc}(t) = [V_s\cos\omega_n t,\, V_s\cos(\omega_n t - 120^\circ), V_s\cos(\omega_n t + 120^\circ)]^T$. Three-phase variables of the network are transformed to a global synchronous DQ frame rotating at the grid nominal frequency $\omega_n$ with initial angle $0^\circ$ [22]. The slack bus voltage equations in global $DQ$ frame are given as

$$v_{1,D} = -\sqrt{2}V_s\sin(0) \tag{9a}$$

$$v_{1,Q} = \sqrt{2}V_s\cos(0) \tag{9b}$$

The source also includes an equivalent system impedance modeling the grid behind the substation. If the short-circuit MVA is given, then the equivalent positive-sequence impedance can be calculated [23]. The impedance can be modeled in the same fashion as a distribution line, as described in the sequel.

### C. Transformer

Consider a grounded wye-grounded wye step-down transformer between bus $i$ and bus $j$. The differential equation pertaining to variables of phase $a$ is obtained by applying KVL between nodes $i$ and $j$ as follows $v_{j,a} = \frac{1}{n_t}v_{i,a} - R_T i_{TX,a} - L_T\dot{i}_{TX,a}$, and likewise for phases $b$ and $c$, where $n_t$ is the transformer ratio, $i_T X$ is the current on the low-voltage side, and $R_T + j\omega_n L_T$ is the leakage impedance referred to the low-voltage side. The dynamics in the $abc$ frame are then converted to the global $DQ$ frame by applying the transformation given in [22, Ch. 3] and are given as follows:

$$\dot{i}_{TX,D} = \frac{1}{L_T}(-R_T i_{TX,D} + \frac{v_{i,D}}{n_t} - v_{j,D}) + \omega_n i_{TX,Q} \tag{10a}$$

$$\dot{i}_{TX,Q} = \frac{1}{L_T}(-R_T i_{TX,Q} + \frac{v_{i,Q}}{n_t} - v_{j,Q}) - \omega_n i_{TX,D} \tag{10b}$$

The dynamic state vector corresponding to the transformer is $\boldsymbol{x}_{\rm T} = \left[i_{{\rm TX},D}, i_{{\rm TX},Q}\right]^T$.

### D. Distribution Line

Consider a line connected between bus $i$ and bus $j$. Self and mutual impedances between phases are respectively denoted as $R_{\phi,\phi} + j\omega_n L_{\phi,\phi}$ and $R_{\phi,\psi} + j\omega_n L_{\phi,\psi}$, where $\phi, \psi \in \{a, b, c\}$ and $\phi \neq \psi$. The present section gives for simplicity the dynamical model of a symmetrical line, where the self and mutual reactances are defined as $L_s = \frac{L_{aa}+L_{bb}+L_{cc}}{3}$ and $L_m = \frac{L_{ab}+L_{bc}+L_{ac}}{3}$ and likewise for the resistances $R_s$ and $R_m$. The differential equation for phase $a$ of the line is obtained from KVL as $v_{i,a} - v_{j,a} = R_s i_{{\rm line},a} + R_m i_{{\rm line},b} + R_m i_{{\rm line},c} + L_s\dot{i}_{{\rm line},a} + L_m\dot{i}_{{\rm line},b} + L_m\dot{i}_{{\rm line},c}$; and likewise for phases $b$ and $c$. The dynamics are converted to the global $DQ$ frame by applying the transformation in [22, Ch. 3]. The resulting equations are

$$\dot{i}_{{\rm line},D} = \frac{1}{L_{\rm line}}(-R_{\rm line} i_{{\rm line},D} + v_{i,D} - v_{j,D}) + \omega_n i_{{\rm line},Q} \tag{11a}$$

$$\dot{i}_{{\rm line},Q} = \frac{1}{L_{\rm line}}(-R_{\rm line} i_{{\rm line},Q} + v_{i,Q} - v_{j,Q}) - \omega_n i_{{\rm line},D} \tag{11b}$$

where $R_{\rm line} + j\omega_n L_{\rm line} = (R_s - R_m) + j\omega_n(L_s - L_m)$ is the positive-sequence impedance of the line. The dynamic state vector corresponding to the line is $\boldsymbol{x}_{\rm line} = \left[i_{{\rm line},D}, i_{{\rm line},Q}\right]^T$.

### E. Load

The differential equations for a load connected to bus $i$ are obtained in the $abc$ frame by applying KVL between bus $i$ and the ground, and then converted to the global $DQ$ frame [5].

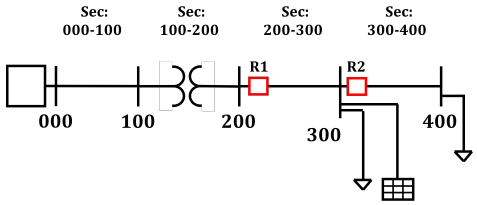


Fig. 3. 5-Bus distribution system.

Supposing a load given by $R_{\text{load}} + j\omega_n L_{\text{load}}$ is connected per phase, the resulting dynamical model is

$$\dot{i}_{\text{load},D} = \frac{1}{L_{\text{load}}}(-R_{\text{load}} i_{\text{load},D} + v_{i,D}) + \omega_n i_{\text{load},Q} \quad (12a)$$

$$\dot{i}_{\text{load},Q} = \frac{1}{L_{\text{load}}}(-R_{\text{load}} i_{\text{load},Q} + v_{i,Q}) - \omega_n i_{\text{load},D} \quad (12b)$$

The dynamic state vector corresponding to the load is $\boldsymbol{x}_{\text{load}} = \left[i_{\text{load},D}, i_{\text{load},Q}\right]^T$.

### F. Algebraic Equations of the System

In this section, the algebraic equations describing relationships among the state variables and the bus voltages are discussed. The algebraic equations include the relations among the currents of the inverter, load, and line are determined by Kirchoff's Current law (KCL) at each bus. In addition, the algebraic equations for transforming the $dq$ synchronous reference frame that is local to each inverter to the global $DQ$ frame are needed. This is because the inverter output currents are represented in the $dq$ frame local to the inverter as shown in the Sections II-A2 and II-A4, and the current injections to each node are represented in the global $DQ$ frame. Note that for simplicity, the equations (13)–(16) are written assuming only one inverter is connected to the system.

The $dq$ frame to $DQ$ frame transformation is given next [6]

$$i_{oD} = \cos(-\delta) i_{od} + \sin(-\delta) i_{oq} \quad (13a)$$

$$i_{oQ} = -\sin(-\delta) i_{od} + \cos(-\delta) i_{oq} \quad (13b)$$

The PCC bus voltage in the inverter's LCL filter dynamics in the Section II-A2 is in $dq$ frame, but the bus voltages of the system are calculated in the global $DQ$ frame. The global $DQ$ frame to $dq$ frame transformation equations are given by [6]

$$v_{\text{PCC},d} = \cos(-\delta) v_{\text{PCC},D} - \sin(-\delta) v_{\text{PCC},Q} \quad (14a)$$

$$v_{\text{PCC},q} = \sin(-\delta) v_{\text{PCC},D} + \cos(-\delta) v_{\text{PCC},Q} \quad (14b)$$

Assume that the inverter and a load are connected to bus $j$. The KCL equation represented in the global synchronous reference frame $DQ$ for the non-faulted bus $j$ is given as

$$i_{ij,DQ} - \sum_{jk \in \mathcal{E}} i_{jk,DQ} = i_{oDQ} - i_{\text{load},DQ} \quad (15)$$

where the left hand side of (15) includes the currents of distribution lines and transformer connected to bus $j$. For a faulted bus $j$ where the inverter and a load are connected, the KCL equation the global $DQ$ frame is stated as

$$i_{ij,DQ} - \sum_{jk \in \mathcal{E}} i_{jk,DQ} = i_{oDQ} - i_{\text{load},DQ} + i_{\text{fault,DQ}} \quad (16)$$

where $i_{\text{fault,DQ}}$ is the fault current. The overall NDAE model of the inverter-based distribution system is summarized as

$$\text{NDAE:} \quad \dot{\boldsymbol{x}} = \boldsymbol{f}(\boldsymbol{x}, \boldsymbol{a}, \boldsymbol{u}) \quad (17a)$$

$$\boldsymbol{0} = \boldsymbol{g}(\boldsymbol{x}, \boldsymbol{a}) \quad (17b)$$

where the dynamic state vector is $\boldsymbol{x} = [\boldsymbol{x}_{\text{PLL}}, \boldsymbol{x}_{\text{LCL}}, \boldsymbol{x}_{\text{CC}}, \boldsymbol{x}_{\text{load}}, \boldsymbol{x}_T, \boldsymbol{x}_{\text{line}}]^T$; the algebraic variables are included in $\boldsymbol{a} = [\{v_{j,D}, v_{j,Q}\}_{j=1}^n, v_{\text{PCC},d}, v_{\text{PCC},q}, i_{oD}, i_{oQ}]^T$; and the vector $\boldsymbol{u} = [P_{\text{ref}}, Q_{\text{ref}}]^T$ is defined. The nonlinear vector-valued functions $\boldsymbol{f}$ and $\boldsymbol{g}$ respectively collect the dynamic and algebraic equations of the system.

## III. Numerical Results for the NDAE Model

In this section, simulation results for the inverter-integrated distribution system NDAE model are presented.

The 5-bus distribution network depicted in Fig. 3 is modeled, consisting of a 13-kV slack bus (designated as 000) with a grid resistance of 0.237 Ω and grid inductance of 0.0082 H. A 13kV/480V grounded wye-grounded wye step-down transformer is connected between buses 100 and 200 with resistance and inductance of 4.15 mΩ and 357 mH, respectively, referred to the low-voltage side. The positive-sequence impedance of the lines is determined from configuration 601 of the IEEE-13 test feeder. Line lengths for lines 000−100, 200−300, and 300−400, are 800 ft, 300 ft, and 300 ft, respectively. We consider constant impedance loads of 650 kW and 15 kvar on bus 300 and 450 kW and 15 kvar on bus 400. A 900-kW inverter at unity power factor is connected on bus 300. The LCL parameters of the inverter are given in Table I. The proportional and integral constants of the PLL block are 0.6 and 20 respectively. The proportional and integral constants of the current controller block are $k_{pc,d} = 10$, $k_{ic,d} = 300$, $k_{pc,q} = 20$, and $k_{ic,q} = 50$. The dynamic factor is set to $K = 2$. MATLAB's `ode15i` solver is used. The NDAE simulation is performed for a timespan of 0.6s and step size 1$\mu$s, and the LLLG fault at bus 400 is applied at $t = 0.3$ sec. The transformation to convert the variables from the $DQ$ global frame to $abc$ is given in [22].

To verify the accuracy of the NDAE simulation, a simulink switching model of the inverter for a solar PV system connected to the 5-bus DN is setup as shown in Fig. 4. The two models are validated with the same LLLG fault at 0.3 sec. The inverter output current and the inverter PCC voltage (bus 300) in $abc$ frame from the NDAE and Simulink simulations are shown in Fig. 5 and Fig. 6, respectively. Under fault conditions, if the change in PCC voltage is more than 5%, the inverter must inject reactive current up to the maximum transient current capacity $I_{\text{limit}}$ according to the DRC control discussed in Section II-A4. From the figures, it is seen that during fault conditions, the inverter injects current close to the maximum transient current limit, but does not exceed this value. The pre- and post-fault PCC voltage and current magnitudes for the NDAE and Simulink simulations are listed in Table II. The inverter output current magnitude error between the NDAE and Simulink simulations is 2.7% (pre-fault) and 5% (post-fault). The PCC voltage magnitude error for the two simulations is 0.2% (pre-fault)

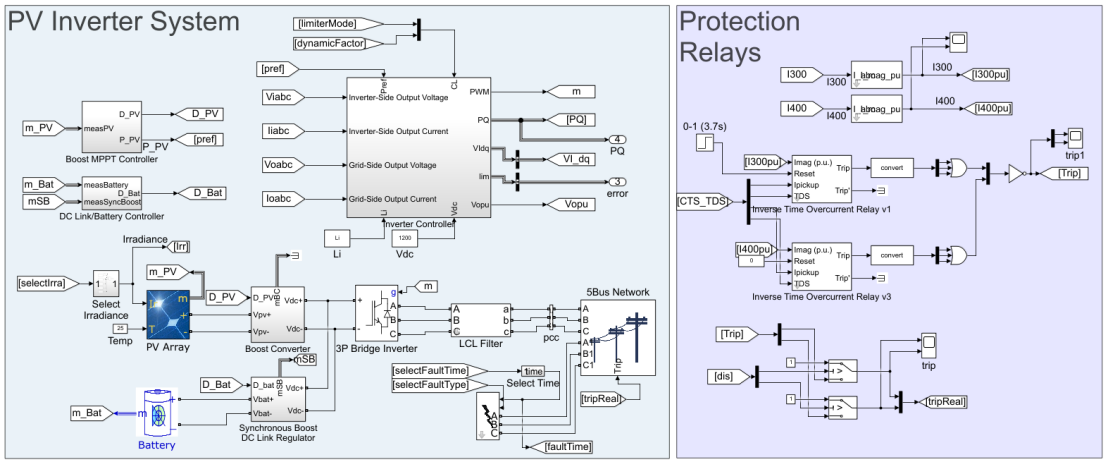


Fig. 4. Simulink PV Inverter and Protection System

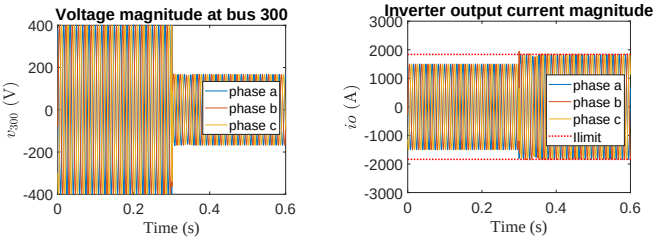


(a) Voltage at Bus 300 (b) Inverter (DRC) output current

Fig. 5. NDAE simulations for a LLLG fault at bus 400.

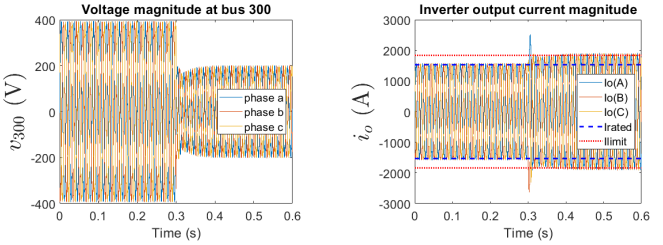


(a) Voltage at Bus 300 (b) Inverter (DRC) output current

Fig. 6. Simulink simulations for a LLLG fault at bus 400.

and 16.5% (post-fault). The post-fault error is due to ripple voltage in Simulink's switching model which was observed to be approximately 28 V.

The inverter-integrated DN model is further extended with protection elements in the sequel.

## IV. Protection System Study

Protection misoperations for OCRs in DNs are well known as blinding and sympathetic-tripping, and they can be categorized as a *failure-to-trip* and as an *undesired-trip*, respectively. There must also be coordination between OCRs, where for every protection zone, there is a designated primary and backup relay. For each primary backup pair, there must be a minimum delay, called the coordination time interval (CTI), which is held in between the operation time of relays. For electronic relays, the CTI is taken as 0.2 s. Discrimination

TABLE I
LCL Filter Parameters

| Lf | Rf | Lc | Rc | Cf | Rd |
|---|---|---|---|---|---|
| 600µH | 1µΩ | 10µH | 1µΩ | 10µF | 1µΩ |

TABLE II
PCC voltage and inverter current magnitudes for NDAE and Simulink simulations

| Fault condition | voltage/current | NDAE | Simulink |
|---|---|---|---|
| Pre-fault | PCC voltage | 394 V | 395 V |
| | Inverter current | 1500 A | 1580 A |
| Post-fault | PCC voltage | 167 V | 200 V |
| | Inverter current | 1825 A | 1800 A |

time is defined as $\Delta t = T_b - T_p$, where $T_b$ and $T_p$ are the operation times of the backup and primary relays, respectively. To coordinate the relays, the following should hold true: $T_b - T_p \geq CTI$, that is the discrimination time should always be greater than or equal to the CTI. The operating time $T$ of a relay is defined in Eq. 18, where $TDS$ is the time dial setting, $I_F$ is the fault current, $I_P$ is the pickup setting, and $A, B, and\ \rho$ are the relay curve characteristic coefficients.

$$T = TDS\left(\frac{A}{\left(\frac{I_F}{I_P}\right)^{\rho} - 1} + B\right) \tag{18}$$

There are two types of blinding misoperations, namely, complete blinding and backup blinding, as shown in Fig. 7. Complete blinding occurs when there is a fault current which is lower in magnitude compared to the pickup setting, meaning the relay will not operate for that fault current. Backup protection blinding can be defined as a *failure-to-trip* within a specified time, for a relay which is acting as backup protection. This time can be referred to as the blinding threshold, and for a well coordinated relay pair, it would hold that $CTI \leq \Delta t \leq t_{blind}$. Blinding is more likely to occur due to increased IBR currents, which reduce the fault current contributed by the upstream line [24, Fig. 4], potentially moving fault currents below the pickup setting, or causing delayed operation past the threshold for blinding. This work

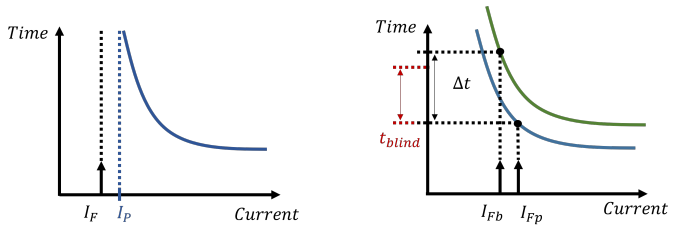


(a) Complete Blinding (b) Backup Blinding

Fig. 7. Blinding Misoperations

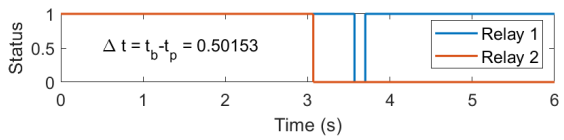


Fig. 8. Operation time with irradiance 1000 $\mathrm{W/m^2}$.

studies the impact of the current limiting model on potential backup blinding events.

## V. DN & PV Inverter System for Protection Study

The distribution network used in this study is same as shown in Fig. 3. The line and load parameters are the same as presented in Section III. The protection elements added to the network are described next. Lines $200-300$ and $300-400$ each have an OCR placed at the sending bus. The relays follow the IEEE Moderately Inverse characteristic with coefficients $A = 0.0515$, $B = 0.114$, and $\rho = 0.02$, taken from IEEE Standard C37.112-201 [25]. The relay on line $200-300$ is R1, and the relay on line $300-400$ is R2. The CT ratio for R1 is $1800:1$, and the ratio for R2 is $900:1$. The pickup currents for R1 and R2 are 1.6 and 3 p.u., respectively, and the TDS is set to 0.131 and 0.05, respectively.

The grid-following inverter, rated at 900 $kW$, is extended with a PV system. The inverter filter parameters are listed in Table I. The active power reference to the inverter comes from the active power output of the PV array. The reactive power setpoint is set to zero during normal operation.

## VI. Simulation Results With Protection System

The distribution network, PV inverter system, and inverter control with current limiting have all been implemented in MATLAB/Simulink with a discrete time-step of 1 $\mu$s. For this study, relay R2 is bypassed, to emulate the failure of the primary protection, and to observe the operation time of the backup protection R1. The complete system is tested by placing a three-phase fault on bus 400, at $t = 3$ s and removing the fault at $t = 3.8$ s. Relay R1 is also reset at $t = 3.8$ s.

Fault ride through standards, such as the German grid code [26], state that inverters must remain connected for up to 0.7 s for a 45% voltage drop, and may require sustained connection for up to 1.5 s depending on the voltage drop. A simple fault ride through strategy is implemented in the PV inverter, where after 150 ms any voltage drop below 30% will cause the inverter to disconnect [26]. If the fault is cleared and the voltage recovers above 90%, the inverter is connected back to the network.

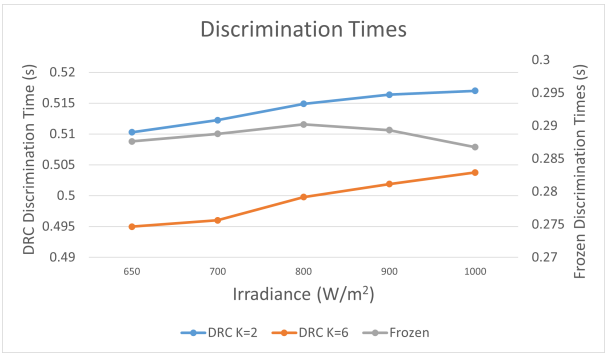


Fig. 9. Discrimination times.

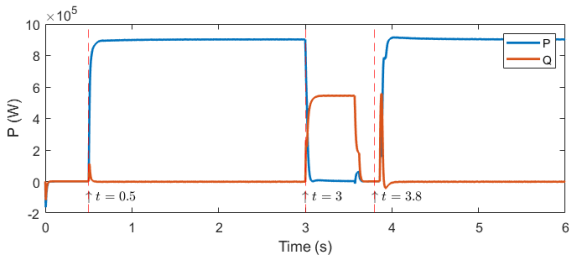


Fig. 10. Power measurement with irradiance 1000 $\mathrm{W/m^2}$ and $K = 6$.

The fault is applied and the discrimination time is recorded, for frozen-control and DRC limiting with dynamic factors $K = 2$ and $K = 6$. The $K$ factor controls the rate of how much reactive current is injected for a given voltage drop, with $K = 2$ and $K = 6$ being the typical minimum and maximum values, respectively. Additionally, the irradiance is varied in five discrete points $\{650, 700, 800, 900, 1000\}$ $\mathrm{W/m^2}$. In the present case study, we consider $t_{blind}$ to be 0.5 s, thus any discrimination time greater than 0.5 s is considered to be backup protection blinding.

Fig. 8 depicts the actual operation times for backup relay R1 (blue) and the expected operation time of primary relay R2 (orange), for the irradiance case of 1000 $W/m^2$; 1 means the breaker is closed and 0 means the breaker is open. Operation time for R2 is said to be expected because the relay is bypassed but the time is still computed and plotted.

Inverter power measurements are shown in Fig. 10. At 0.5 s the inverter is connected to the network and the active power goes to 900 kW. At 3 s, the fault is applied and the reactive power injection by the inverter can be observed. At 3.56 s, the backup relay opens and the voltage drops below 30%, at which point the inverter stops operating. After 3.8 s, when the fault is removed and the breaker is reset (closed), the voltage goes above 90% and the inverter is connected again.

Results of the discrimination times for frozen control and DRC limiting are shown in Fig. 9, where the left axis has the DRC discrimination times and the right y-axis has the frozen discrimination times. For frozen control, the discrimination times are all between the CTI and $t_{blind}$, 0.2 s and 0.5 s respectively, and it can be said that the relay settings are reasonably coordinated. Both DRC lines, $K = 2$ and $K = 6$, are following the same trend, where as the irradiance

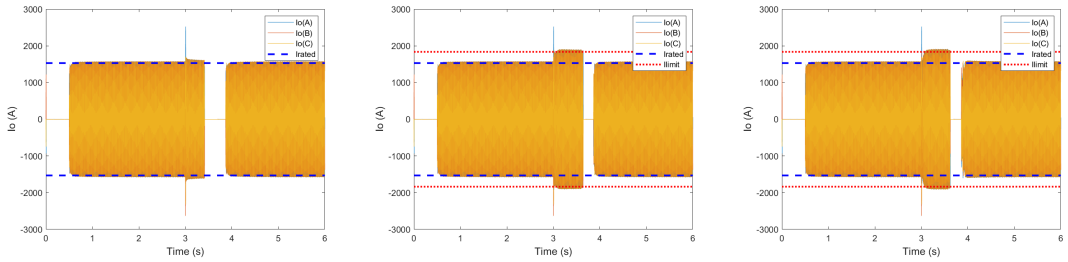


(a) Frozen (b) Dynamic $K = 2$ (c) Dynamic $K = 6$

Fig. 11. Inverter output current for different current limiting modes

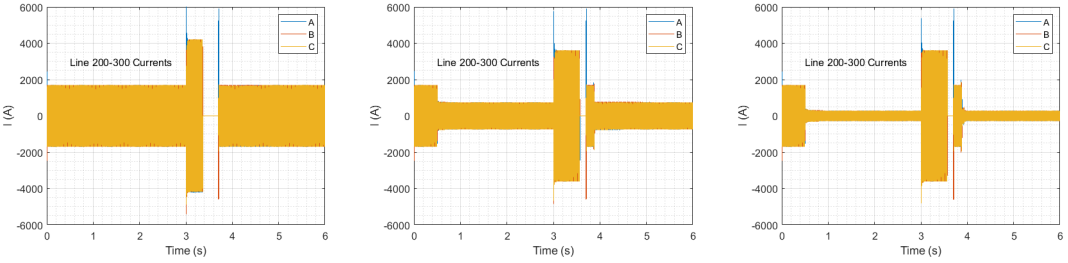


(a) No Inverter (b) Inverter, 650 $\mathrm{W/m^2}$, $K = 6$ (c) Inverter, 1000 $\mathrm{W/m^2}$, $K = 6$

Fig. 12. Impact of the inverter current on the upstream line $200 - 300$

increases, discrimination time also increases. This is because as irradiance increases, so does the PV current contribution, which decreases the current contributed through line $200-300$. The trend of the line for $K = 2$ looks similar to that of $K = 6$, with a vertical shift upwards. Higher currents, in the case of $K = 6$, will result in faster operation times of the backup relay, thus lower discrimination times. Conversely, lower currents, in the case of $K = 2$, will result in delayed or longer operation times, thus increased discrimination times. For dynamic factor $K = 6$ and the last two irradiance points, the discrimination time has exceeded the blinding threshold, potentially affecting the safe DN operation. With dynamic factor of $K = 2$, the relay settings under all irradiance cases have resulted in blinding. From these results, it is evident that protection system which is coordinated through fault analysis performed with simplified fault response models, may face misoperations when the actual nonlinear fault response occurs in the network. Further, it is concluded that considering the dynamic factor setting is also critical in the fault analysis used for protection settings coordination.

The transient responses for frozen-control, and dynamic-control with $K = 2$ and $K = 6$ modes, are shown in Fig. 11. In Fig. 11a, the response for frozen control, the current magnitude during the fault remains very close to the prefault magnitude. In Figs. 11b and 11c, under DRC control, it can be seen the current magnitude during fault is increased in compared to the prefault magnitude. Fig. 12 shows the current through line $200-300$, without the inverter, and with the inverter under irradiance values of 650 $\mathrm{W/m^2}$ and 1000 $\mathrm{W/m^2}$. The impact of the inverter current on the upstream line $200 - 300$ is evident by comparing the no inverter plot to the ones with inverter. With the inverter connected, the upstream current is reduced, which is the cause of the delayed operation of backup relay R1.

## VII. Conclusions and Future Work

A nonlinear differential and algebraic equation model for inverters with DRC limiting connected to a distribution network under faulted conditions is developed. The PV inverter control system with DRC limiter has been implemented in Simulink and coupled with a 5-bus distribution network, which has a protection system consisting of two OCRs. Discrimination times are recorded for various irradiance scenarios for fault response following frozen control as well as dynamic control with $K = 2$ and with $K = 6$. It is observed that increasing irradiance causes increased discrimination time between primary and backup relays for dynamic limiting mode. Further, if $K$ factor for the inverter current limiter is changed, discrimination times can increase, potentially causing blinding scenarios. It is thus of critical importance to properly model the current limiter when performing fault analysis, to protect the network from potential blinding events.

Future research includes analysis of larger networks, introducing unbalanced faults, and investigating DRC limiter strategies with simultaneous positive- and negative-sequence current control.

## References

[1] C. A. Plet, M. Graovac, T. C. Green, and R. Iravani, "Fault response of grid-connected inverter dominated networks," in *IEEE PES general meeting*. IEEE, 2010, pp. 1–8.

[2] M. E. Baran and I. El-Markaby, "Fault analysis on distribution feeders with distributed generators," *IEEE transactions on power systems*, vol. 20, no. 4, pp. 1757–1764, 2005.

[3] S. H. Horowitz and A. G. Phadke, *Power System Relaying*. John Wiley & Sons, Ltd, 2008.

[4] D. Lagos, V. Papaspiliotopoulos, G. Korres, and N. Hatziargyriou,

"Microgrid Protection Against Internal Faults," *IEEE Power and Energy Magazine*, vol. 19, no. 3, pp. 20–35, 2021.

[5] M. Rasheduzzaman, J. A. Mueller, and J. W. Kimball, "An accurate small-signal model of inverter-dominated islanded microgrids using (dq) reference frame," *IEEE Journal of Emerging and Selected Topics in Power Electronics*, vol. 2, no. 4, pp. 1070–1080, 2014.

[6] ——, "Reduced-order small-signal model of microgrid systems," *IEEE Transactions on Sustainable Energy*, vol. 6, no. 4, pp. 1292–1305, 2015.

[7] J. A. Mueller, *Small-signal modeling of grid-supporting inverters in droop controlled microgrids*. Missouri University of Science and Technology, 2014.

[8] N. Kroutikova, C. A. Hernandez-Aramburo, and T. C. Green, "State-space model of grid-connected inverters under current control mode," *IET Electric Power Applications*, vol. 1, no. 3, pp. 329–338, 2007.

[9] W. Du, F. K. Tuffner, K. P. Schneider, R. H. Lasseter, J. Xie, Z. Chen, and B. Bhattarai, "Modeling of grid-forming and grid-following inverters for dynamic simulation of large-scale distribution systems," *IEEE Transactions on Power Delivery*, vol. 36, no. 4, pp. 2035–2045, 2020.

[10] G. Kou, L. Chen, P. Vansant, F. Velez-Cedeno, and Y. Liu, "Fault Characteristics of Distributed Solar Generation," *IEEE Transactions on Power Delivery*, vol. 35, no. 2, pp. 1062–1064, 2020.

[11] A. Haddadi, E. Farantatos, I. Kocar, and U. Karaagac, "Impact of inverter based resources on system protection," *Energies*, vol. 14, no. 4, pp. 1–21, 2021.

[12] A. K. Barnes, J. E. Tabarez, A. Mate, and R. W. Bent, "Optimization-based formulations for short-circuit studies with inverter-interfaced generation in powermodelsprotection. jl," *Energies*, vol. 14, no. 8, p. 2160, 2021.

[13] A. Mathur, B. Das, and V. Pant, "Fault analysis of unbalanced radial and meshed distribution system with inverter based distributed generation (ibdg)," *International Journal of Electrical Power & Energy Systems*, vol. 85, pp. 164–177, 2017.

[14] I. Kim, "A calculation method for the short-circuit current contribution of current-control inverter-based distributed generation sources at balanced conditions," *Electric Power Systems Research*, vol. 190, p. 106839, 2021.

[15] R. Furlaneto, I. Kocar, A. Grilo-Pavani, U. Karaagac, A. Haddadi, and E. Farantatos, "Short circuit network equivalents of systems with inverter-based resources," *Electric Power Systems Research*, vol. 199, p. 107314, 2021.

[16] N. Tleis, *Power Systems Modelling and Fault Analysis: Theory and Practice*, 2nd ed. Elsevier, 2019.

[17] A. Fidigatti and E. Ragaini, "Effect of harmonic pollution on low voltage overcurrent protection," *ICHQP 2010 - 14th International Conference on Harmonics and Quality of Power*, 2010.

[18] K. A. Wheeler, S. O. Faried, and M. Elsamahy, "Fault impedance effects on distributed generation influences in overcurrent protection," in *2017 IEEE Manchester PowerTech, Powertech 2017*. IEEE, 2017.

[19] E. Sorrentino and T. Marcano, "Experimental method to summarize the effect of transformer inrush currents on a digital overcurrent relay," *2020 Ieee Andescon, Andescon 2020*, 2020.

[20] M. Zadeh, P. K. Mansani, and I. Voloh, "Impact of Inverter-based Resources on Impedance-based Protection Functions," *2021 74th Conference for Protective Relay Engineers, CPRE 2021*, pp. 1–6, 2021.

[21] H. S. Samkari and B. K. Johnson, "Impact of Distributed Inverter-Based Resources on Incremental Quantities-Based Protection," *IEEE Power and Energy Society General Meeting*, vol. 2021-July, 2021.

[22] P. C. Krause, O. Wasynczuk, S. D. Sudhoff, and S. D. Pekarek, *Analysis of electric machinery and drive systems*. John Wiley & Sons, 2013.

[23] W. H. Kersting, *Distribution system modeling and analysis*, 4th ed. CRC press, 2018.

[24] P. Mishra, A. Kumar Pradhan, and P. Bajpai, "Adaptive Relay Setting for Protection of Distribution System with Solar PV," in *2018 20th National Power Systems Conference, NPSC 2018*, vol. 2, no. 1, 2018, pp. 1–5.

[25] "IEEE Standard for Inverse-Time Characteristics Equations for Overcurrent Relays," Institute of Electrical and Electronics Engineers, Standard, Dec. 2019. [Online]. Available: https://ieeexplore.ieee.org/document/8635630

[26] E. Troester, "New German grid codes for connecting PV systems to the medium voltage power grid," *2nd International workshop on concentrating photovoltaic power plants: optical design, production, grid connection*, pp. 9–10, 2009.